ACS PHYSICAL CHEMISTRY Au
AN OPEN ACCESS JOURNAL OF THE AMERICAN CHEMICAL SOCIETY

pubs.acs.org/physchemau

Article

New Tools for Taming Complex Reaction Networks: The Unimolecular Decomposition of Indole Revisited

Diego Garay-Ruiz, Moises Álvarez-Moreno, Carles Bo,* and Emilio Martínez-Núñez*

Cite This: *ACS Phys. Chem Au* 2022, 2, 225−236

Read Online

ACCESS | Metrics & More | Article Recommendations | Supporting Information

ABSTRACT: The level of detail attained in the computational description of reaction mechanisms can be vastly improved through tools for automated chemical space exploration, particularly for systems of small to medium size. Under this approach, the unimolecular decomposition landscape for indole was explored through the automated reaction mechanism discovery program AutoMeKin. Nevertheless, the sheer complexity of the obtained mechanisms might be a hindrance regarding their chemical interpretation. In this spirit, the new Python library *amk-tools* has been designed to read and manipulate complex reaction networks, greatly simplifying their overall analysis. The package provides interactive dashboards featuring visualizations of the network, the three-dimensional (3D) molecular structures and vibrational normal modes of all chemical species, and the corresponding energy profiles for selected pathways. The combination of the joined mechanism generation and postprocessing workflow with the rich chemistry of indole decomposition enabled us to find new details of the reaction (obtained at the CCSD(T)/aug-cc-pVTZ//M06-2X/MG3S level of theory) that were not reported before: (i) 16 pathways leading to the formation of HCN and NH_3 (via amino radical); (ii) a barrierless reaction between methylene radical and phenyl isocyanide, which might be an operative mechanism under the conditions of the interstellar medium; and (iii) reaction channels leading to both hydrogen cyanide and hydrogen isocyanide, of potential astrochemical interest as the computed HNC/HCN ratios greatly exceed the calculated equilibrium value at very low temperatures. The reported reaction networks can be very valuable to supplement databases of kinetic data, which is of remarkable interest for pyrolysis and astrochemical studies.

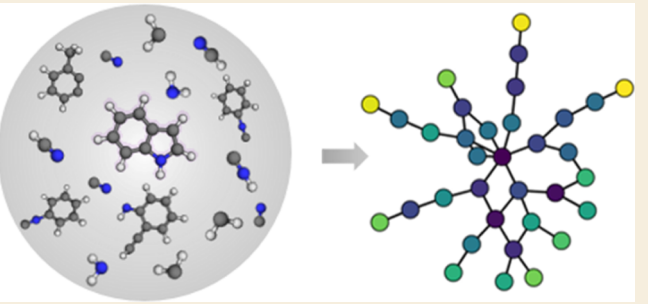

KEYWORDS: *indole, reaction networks, automated mechanism discovery, pyrolysis, astrochemistry, data analysis, visualization*

1. INTRODUCTION

Over the last decades, much effort has been devoted to the development of advanced computational methods to probe reaction mechanisms. These methods range from saddle points search algorithms[1−23] to automated protocols for chemical reaction space exploration.[24−64] The vast majority of automated methods leverage chemical heuristics and/or reactive molecular dynamics (MD) simulations to reveal complex reaction networks (RXNets). Some of these ideas have been implemented in computer programs like *autodE*,[65] *AutoMeKin*,[66] *ChemDyME*,[67] *ChemTraYzer*,[68] *GRRM*,[69] *KinBot*,[70] and *RMG*.[71] These methods are particularly effective with chemical systems of small to medium size, depending on the computational resources that are available. For an increasing number of cases, very detailed mechanistic descriptions can be obtained, going further beyond what could be attained with manual explorations of the potential energy surface. In this way, the decomposition of indole, a heterocyclic aromatic compound with a structure consisting of a pyrrole ring fused to a benzene ring, arises as an interesting target for this kind of automated search: it is a relatively small molecule (12 atoms), but still its unimolecular decomposition pathways show a rich reaction landscape.

AutoMeKin is an open-source program to automate reaction mechanism prediction.[66] Both heuristics-based and MD-based methods are implemented in the code, making it very flexible and efficient. The resulting RXNets typically contain from hundreds to thousands of intermediates and TSs,[62,72−81] which makes the analysis very tedious. To alleviate this problem, we present a collection of new processing and visualization tools (named *amk-tools*) that parse *AutoMeKin's* output and create interactive plots that enable user-friendly navigation of RXNets. This enhanced network exploration provides the user a direct insight into the chemistry of the studied system, connecting the network topology with the chemical structures of the corresponding intermediates and transition states.

Received: December 14, 2021
Revised: January 25, 2022
Accepted: January 25, 2022
Published: February 4, 2022

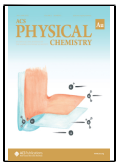

https://doi.org/10.1021/acsphyschemau.1c00051
ACS Phys. Chem Au 2022, 2, 225−236

The new postprocessing tools were applied to the mechanisms of indole decomposition, owing to their combination of chemical interest and remarkable complexity. Indole is present in coal tar being one of its N-containing compounds.[82] Thus, its decomposition channels in a pyrolytic environment are important for the study of coal combustion. Liu et al.[83] have recently employed DFT methods to map the dissociation mechanisms leading to HCN and NH_3, which are the main volatile precursors of NOx.[84] Our analysis of the decomposition channels will also be focused on the HCN and NH_3 formation mechanisms to compare with the previous DFT results.

Additionally, barrierless routes for indole formation can be sought by analyzing the decomposition channels in reverse. Probing barrierless mechanisms leading to the formation of indole from neutral molecular species, which are typically found in low-temperature interstellar environments, could be of great interest in astrochemistry. Although indole (C_8H_7N) has not yet been detected in the interstellar medium (ISM), microwave data have been recently recorded with the aim of supporting its unambiguous identification in the ISM.[85] Furthermore, both methylene (CH_2)[86] and benzonitrile[87] (C_6H_5CN) have been detected in the ISM. In this respect, the new toolset presented herein can help identify the routes of formation of indole from the fragments CH_2 and C_6H_5CN.

In addition to this, photolysis of indole can lead to HCN after the initially prepared excited state proceeds by internal conversion to the ground state.[88,89] Then, if the molecule is present in the ISM, photodissociation of indole may be a viable source of HCN and HNC, which are well-known constituents of the ISM.[90] For this reason, studying the elimination kinetics of these products can help explain the unexpected HNC/HCN branching ratio found in the ISM.[91,92]

The results obtained with AutoMeKin will provide the dissociation dynamics in the ground electronic state only. The full picture including electronic excited states and nonadiabatic chemistry can be studied with dedicated software like GRRM[69] or the nonadiabatic nanoreactor.[93]

2. METHODOLOGY

2.1. AutoMeKin

AutoMeKin stands for *Auto*mated *Me*chanisms and *Kin*etics, and it is an automated protocol to discover chemical reaction mechanisms and simulate the kinetics at the reaction conditions of interest. Although the method was originally designed to find transition states (TSs) from reactive molecular dynamics (MD) simulations,[39,40] several new tools have been incorporated throughout the past few years.[66,94] The current pipeline consists of three steps:

(1) Exploration of reaction mechanisms through MD simulations or chemical knowledge-based algorithms.
(2) Use of Graph Theory algorithms to build the reaction network (RXNet).
(3) Kinetics simulations.

The new capabilities include a rare-event acceleration MD algorithm, a new method to explore noncovalently bound structures, heuristics-guided explorations of reaction mechanisms, a new reactive event detection algorithm, statistical analysis of the RXNet, and a web application.[66] Most of these new features belong to the first step of the above pipeline.

The second step consists of the construction of the RXNet. This is initiated with IRC calculations to connect each TS with a reactant/product pair, which are then followed by optimizations of the minima. Finally, all possible connections between every pair of minima are built using the Python package NetworkX.[95] These networks of chemical reactions can be studied by Graph Theory, where a node corresponds to a minimum while an edge represents a TS connecting two nodes (with or without saddle points). The use of NetworkX also facilitates the study of the structure of the networks by identifying the presence of hubs (highly connected nodes) and providing the shortest paths between reactants and products.

2.2. amk-tools

The new methods implemented in the mechanism search workflow enable an efficient construction of reaction networks. However, the obtained RXNets may be very complex, which requires advanced tools to facilitate their visualization and analysis. While experienced users may employ custom scripts to process the computed networks, a more user-friendly approach would facilitate the extension of this kind of automated methods to a larger part of the community. Moreover, there is also a growing interest in digital repositories to store and share computational chemistry results, such as ioChem-BD.[96,97] While the individual calculations could, in principle, be seamlessly uploaded to a database, the picture painted by the (likely abundant) data will not be complete without the underlying network structure. To fill these gaps, we developed the *amk-tools*[98] package, a Python library designed to *parse*, *process*, and *transform* the reaction networks explored by *AutoMeKin*, whose basic workflow is outlined in Figure 1.

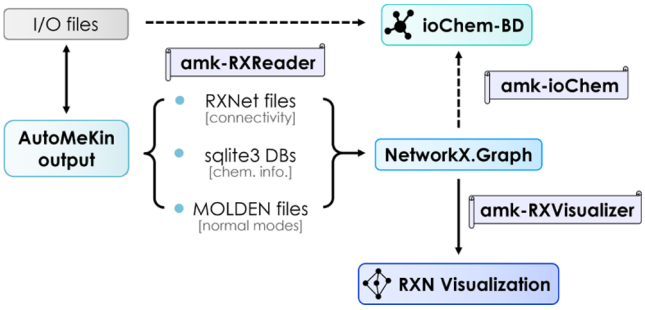

Figure 1. Data pipeline for *amk-tools*, employing *amk-RXReader* to parse *AutoMeKin* output to a graph object that then can be passed to (i) the *amk-ioChem* module for the automated upload of the network and associated calculations to the ioChem-BD platform and (ii) the *amk-RXVisualizer* module for the interactive visualization of reaction networks.

The *amk-ioChem* module provides a protocol to upload all calculations in a reaction network to ioChem-BD, through the corresponding shell client, and simultaneously generate the structure of the reaction network, which can be directly regenerated in the ioChem-BD platform.

On the other hand, the *amk-RXVisualizer* module is designed to generate interactive visualization dashboards in HTML format linking the network topology with the corresponding chemical structures, energies, and vibrational modes. The visualizations, powered by the Bokeh[99] library, allow the end user to easily explore and share the resulting reaction networks.

These dashboards present three main elements, as shown in Figure 2: (i) network visualization, allowing zooming and

https://doi.org/10.1021/acsphyschemau.1c00051
ACS Phys. Chem Au 2022, 2, 225−236

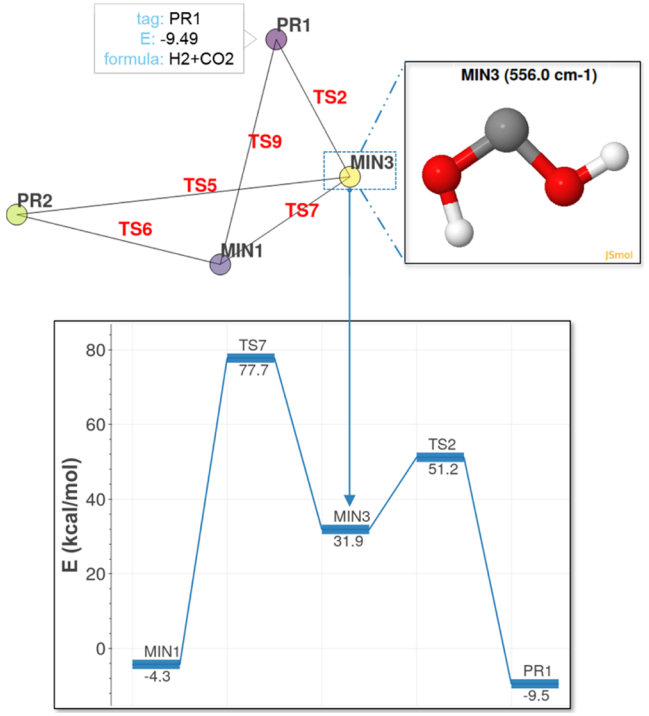

Figure 2. Main elements for interactive visualization dashboards: (i) reaction network, (ii) molecular visualizer, and (iii) energy profile visualizer. The formic acid decomposition network from *AutoMeKin* example runs is depicted as a reference.

panning across the network, selecting species, and hovering over nodes and edges to obtain information; (ii) 3D molecule visualization, via JSMol, for selected molecules and vibrational normal modes; and (iii) energy profile visualization, plotting energies for selected pathways across the network, which can be filtered according to threshold energies or involved molecules. A more detailed explanation of the available controls and functionalities is provided in the accompanying GitHub repository. The visualization dashboards can be generated either through a simple command-line tool or through custom Python scripts if a more detailed preprocessing of the input network is necessary. The reaction energy profiles are generated through path traversals across the main network between a set of source nodes and a set of target nodes. An exhaustive search of all possible paths across the network can also be performed, but both the number of resulting paths and the calculation time scale rapidly with the size of the network.

2.3. Test Case

To test the new tool, the unimolecular dissociation channels of indole and the radical resulting from breakage of the N−H bond have been studied because of their interest in coal combustion and astrochemistry, as explained above. Following the nomenclature of a previous computational study on this system, the radical is named indole-a: the corresponding structures are shown in Scheme 1.[83]

Scheme 1. Chemical Structures of Indole and Indole-a

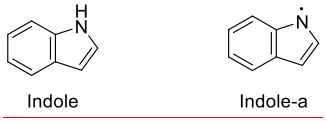

The low-level calculations employed to explore the reaction mechanisms comprise 30 iterations of *AutoMeKin*'s low-level workflow: MD simulations, RXNet construction, and kinetics simulations.[66] Each set of the MD simulations involves 500 trajectories integrated for 0.5 ps, or until dissociation occurs. TSs with imaginary frequencies lower than 200i cm^{-1} are discarded, and the kinetics simulations employ an excitation energy of 250 kcal/mol. This large value was selected to include pathways playing an important role in the pyrolysis of indole.[83] Screening of duplicate structures and identification of fragments is done inside the program using the following threshold values for MAPEmax, BAPEmax, and eigLmax: 0.008, 2.5, and 0.1, respectively.[94] Details on the meaning and significance of these parameters are provided in the Supporting Information (Section 6).

The automated procedure followed in this work involves a hierarchy of electronic structure methods: (a) the semi-empirical PM7 method[100] (Level1) is employed in the low-level workflow explained above, (b) HF/3-21G (Level2) is subsequently used to reoptimize the PM7 structures for fast screening of the channels of interest, and finally (c) the CCSD(T)/aug-cc-pVTZ//M06-2X/MG3S level of theory (Level3) is employed to study the HCN, CN, and NH_2 dissociation channels, as well as a barrierless mechanism leading to methylene, which could be of interest in astrochemistry. Level1, Level2, and Level3 calculations were carried out with MOPAC2016,[101] Gaussian09,[102] and Gaussian16,[103] respectively. The HNC/HCN branching ratio is also calculated using RRKM theory[104] and chemical master equation calculations implemented in AutoMeKin's kinetics module.

Since many dissociation pathways of the present work do not present a barrier, a new algorithm has been implemented to include barrierless dissociation pathways in our workflow. The possible barrierless bond-breaking events are probed by constrained dynamics simulations. If the dissociation leads to two fragments of energies below a given threshold, and no alternative path exists between the two nodes, the event is regarded as barrierless. A more detailed description of the protocol implemented in the new module is available in the Supporting Information. Additionally, for this system, C−H and N−H bond dissociations were not allowed by restricting the minimum number of neighbors for the hydrogen atoms to one.[66]

3. RESULTS AND DISCUSSION

3.1. Convergence of Results

Figure 3 shows the branching ratios obtained from indole and indole-a for the predominant channels (presenting a barrier) using an excitation energy of 250 kcal/mol, assessing the kinetic convergence over the iterative TS search procedure. Product yields were obtained using AutoMeKin's kinetics module, which utilizes harmonic RRKM theory[104] for the rate constants and kinetic Monte Carlo (KMC)[105] for the chemical master equation. Although the analysis of Figure 3 is only for testing purposes, the results already show some channels (like HCN and C_2H_2) that also appear in an experimental study of the thermal decomposition of indole in the temperature range 1050−1650 K.[106]

While for indole the branching ratios level off rather quickly (at ∼10 iterations), for the radical, a small uptick is observed at 23 iterations. At any rate, the results shown in Figure 3 seem to

https://doi.org/10.1021/acsphyschemau.1c00051
ACS Phys. Chem Au 2022, 2, 225−236

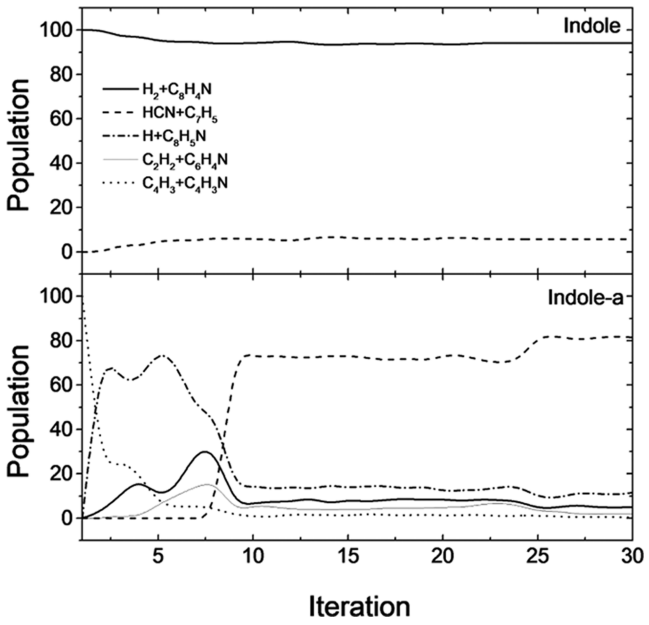

Figure 3. Branching ratios for the major decomposition channels (that go over a barrier) of indole and indole-a at 250 kcal/mol using Level1. The abscissa shows the iterations of the low-level workflow.

indicate that the workflow was successful in mapping the kinetically relevant pathways.

3.2. Properties of the RXNets

Reaction networks obtained in this work are rather complex with hundreds of nodes (intermediates) and thousands of edges (transition states), as seen in Figure 4. Table 1 shows some properties of the RXNets obtained at Level1 and Level2 for both indole and the radical indole-a (additional details can be found in the Supporting Information).

Table 1. Some Properties of the Reaction Networks[a]

	indole		indole-a	
	Level1	Level2	Level1	Level2
nodes	909	863	398	258
edges	2178	1846	1416	700
average shortest path length	3.8 (4.6)	4.1 (5.0)	3.0 (3.3)	3.4 (3.5)
average clustering coefficient	0.17 (0.005)	0.13 (0.005)	0.23 (0.018)	0.15 (0.021)

[a]Numbers in parentheses refer to the corresponding values for a random (Erdös–Rényi) network with the same number of nodes and edges.

Reaction networks in chemistry typically display the so-called "small-world" behavior,[62,66,107,108] where pairs of nodes are connected through a small number of edges, *i.e.*, networks present small values for the average shortest path lengths. Table 1 shows that our computed average shortest path lengths are shorter than those for the corresponding random networks, mimicking the behavior of other networks in chemistry.

The proportion of interlinking between neighbors is characterized by the clustering coefficient, which becomes larger in the so-called "scale-free" networks than in random networks of equivalent size. The results obtained in Table 1 indicate that our networks are scale-free (as known for previous chemical networks[62,66]) presenting a hierarchy of nodes with a small proportion (called hubs) being highly connected, more nodes with fewer connections, down to nodes with only a few connections.

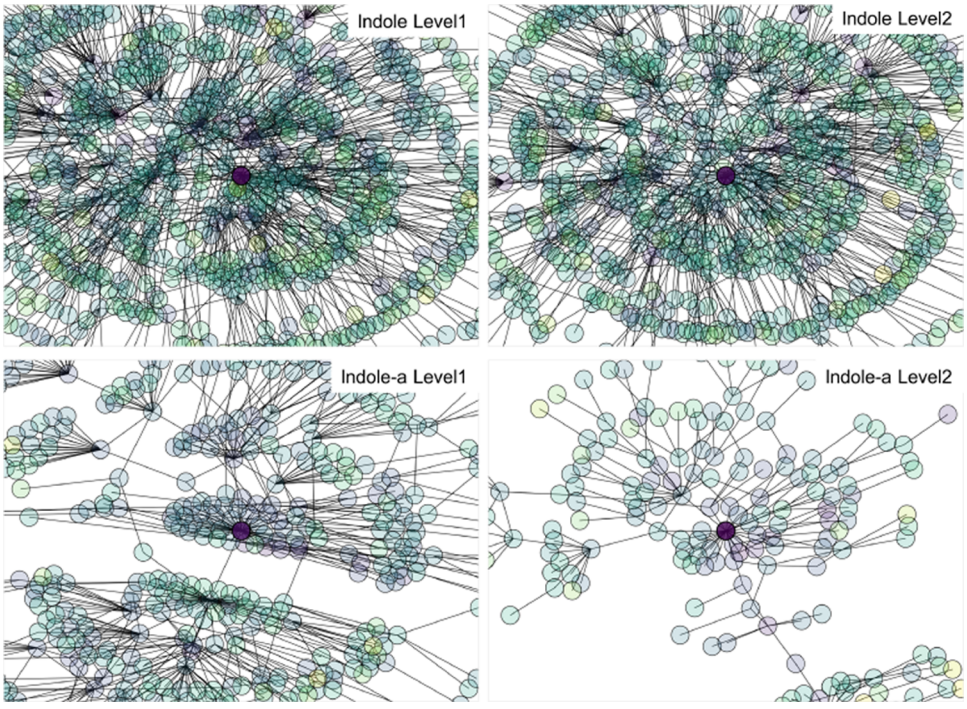

Figure 4. Graphical representation of the RXNets obtained at Level1 and Level2 for indole and indole-a. The networks only display the vicinity of the global minima, which are located at the center of the RXNets and highlighted in purple. Node colors depend on energy through the "viridis" colormap, ranging from purple (low energy) to yellow (high energy).

https://doi.org/10.1021/acsphyschemau.1c00051
ACS Phys. Chem Au 2022, 2, 225–236

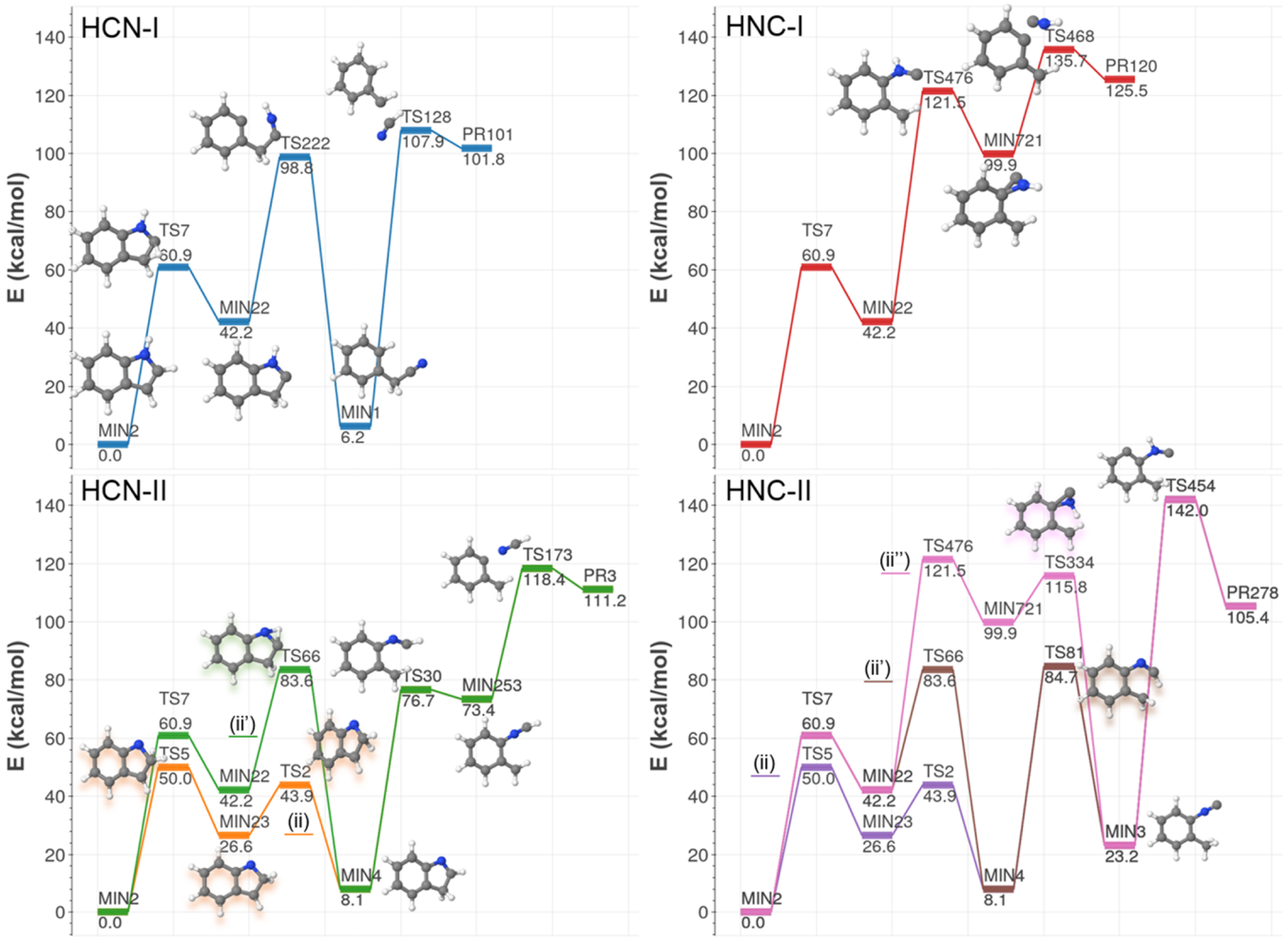

Figure 5. Level3-calculated energy profiles for HCN and HNC elimination. The displayed channels were obtained after filtering those obtained at Level2 using a threshold energy of 150 kcal/mol and a maximum number of elementary steps of 4.

3.3. HCN Formation Channels

Among all of the decomposition channels of indole, those leading to the formation of HCN and NH_3 are of special relevance to atmospheric chemistry because these molecules are the main volatile precursors of NOx.[84] Very recently, Liu et al. studied the formation mechanisms of these two species at the DFT B3LYP/6-31G(d,p) level of theory,[83] and it could be of interest to compare their results with those obtained in this study. With regard to the formation of hydrogen cyanide, Liu et al. proposed five pathways leading to the formation of cyano radical, which subsequently needs to react with an atomic hydrogen to form HCN.[83]

From the Level2-calculated complete RXNet, HCN and CN formation routes were sought through the current postprocessing pipeline. Using cutoff values of 5 and 250 kcal/mol for the maximum number of elementary steps and maximum energy of the highest TS, respectively, 195 HCN elimination pathways were obtained with 281 different stationary points involved. However, to keep the computational cost within the limit, we decided to filter the HCN channels using cutoffs of 4 and 150 kcal/mol, which results in the 7 pathways and 21 different stationary points described below. Notwithstanding that, the computational cost of all Level3 calculations (including the remaining channels described below) was ∼4 years of CPU time.

To label the numerous reaction channels found in the reaction network, we named each as FRAG(-*a*-)-X, where FRAG is the chemical formula of the obtained fragment, X is a Roman numeral, and -a- refers to indole-a decomposition processes. Some of the channels group together several individual pathways having the same length, sharing intermediates and leading to the exact same fragments.

Figure 5 shows the direct HCN elimination channels found in this study with the above constraints. Routes leading to both hydrogen cyanide (HCN-I and HCN-II) and to hydrogen isocyanide (HNC-I and HNC-II) were found. These direct pathways of HCN(HNC) formation were overlooked in the previous study[83] probably because they are difficult to envision using by-hand searches.

All HCN(HNC) elimination channels of Figure 5 have in common an initial hydrogen migration leading to MIN22 or MIN23 intermediates. Then, all routes proceed with a ring-opening process before the elimination step, with the longer ones (HCN-II and HNC-II) involving additional H migrations with respect to the three-step pathways (HCN-I and HNC-I). Table 2 shows the amount of HCN(HNC) formed via the four routes of Figure 5 at four excitation energies. The excitation energies were selected to match photon wavelengths of radiation present in the ISM, and therefore the subsequent discussion is relevant to astrochemistry (see Section 3.5). The table shows that HCN formation is much more abundant than

https://doi.org/10.1021/acsphyschemau.1c00051
ACS Phys. Chem Au 2022, 2, 225−236

Table 2. Product Yields (in %) for the HCN(HNC) Elimination Channels of Figure 5[a]

energy (kcal/mol)	HCN-I	HNC-I	HCN-II	HNC-II
150	96.17	0.00	3.83	0.00
180	67.24	0.01	32.71	0.00
200	43.88	0.07	56.05	0.00
235	21.26	0.26	78.47	0.01

[a]The results are obtained after averaging the product abundances of 10 independent KMC runs using 10^4 molecules.

the formation of HNC with HNC/HCN branching ratios ranging from 0 to 3×10^{-3}. The three-step HCN-I pathway is the predominant one at the lowest excitation energy, with HCN-II taking over as the excitation energy increases, which can be explained by an entropic effect. The finding of mechanisms leading to both species HCN and HNC has implications in astrochemistry as discussed below.

Two previously unreported additional hydrogen cyanide elimination channels from indole-a (HCN-a-I and HCN-a-II) were found using the same cutoffs as above (Figures S1 and S2). Both routes consist of four steps with significant ring rearrangements on indole-a, with HCN-a-I being enthalpically more favorable due to lower barrier heights.

CN elimination paths were also studied and compared with the results from Liu et al.,[83] who proposed five different CN-forming pathways. While two of these pathways (path-b and path-c) involve alternative indole radicals that we have not considered in this work, the other three (path-1, path-3, and path-a) were reproduced through our current protocol, together with some additional routes as summarized in Table 3.

Table 3. HCN Formation Pathways Predicted by AutoMeKin in Comparison with the Previous DFT Study

Liu et al.[83]	this work[a]
	Direct Paths
[b]	HCN-I, HCN-II *(x2)*, HNC-I, HNC-II *(x3)*
[b]	HCN-a-I, HCN-a-II
	Paths via CN Radical
Path-1	CN-i
Path-3	CN-i′
Path-a	CN-a-II
[b]	CN-II, CN-III *(x3)*, CN-a-I, CN-a-III

[a]Pathways are named FRAG(-*a*-)-X, where FRAG is the chemical formula of the obtained fragment, X is a Roman numeral, and -a- refers to indole-a. Labels of products (PR) and minima (MIN) correspond to the RXNet obtained at Level3 from indole/indole-a. Numbers within parentheses indicate the number of individual pathways for channels containing more than one reaction path. [b]Not found in the previous DFT study.

Starting from indole, three CN-forming channels (through six unique pathways) were found (Figures S3 and S4): CN-I (which engulfs the paths CN-i, analogous to path-1 and CN-i′, matching path-3), CN-II, and CN-III. However, compared to CN-I, these two newly reported routes involve one additional step. All of these pathways share several intermediates with the HCN(HNC)-forming routes shown in Figure 5, highlighting the large interconnectivity of the nodes in the network.

For the decomposition of the indole-a radical, we found three channels leading to cyano radical, producing the same fragments but with different lengths. CN-a-I (Figure 6) is a novel, two-step channel involving a concerted transition state

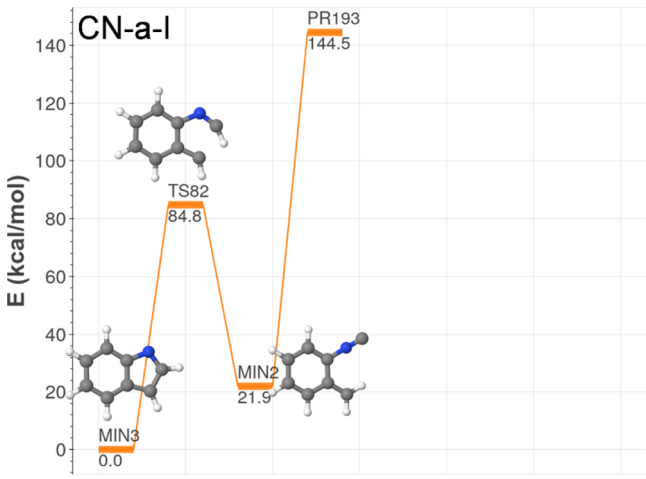

Figure 6. Level3-calculated energy profile for one of the new CN elimination pathways from indole-a found in this study. Two additional pathways involving three and four steps, respectively, are displayed in Figure S5. The channels were obtained after filtering those obtained at Level2 using a threshold energy of 150 kcal/mol and a maximum number of elementary steps of 4.

for hydrogen transfer and C−C breakage, which should be kinetically favored. CN-a-II (Figure S5, blue) matches path-a from the previous work, while CN-a-III (Figure S5, green) is a longer, higher-energy route with minor contribution to the reactivity.

3.4. NH_3 Formation Channels

Compared to HCN formation, the number of pathways leading to ammonia (Figure 7) is considerably reduced. Our results indicate that NH_3 cannot be directly formed from indole radical, but instead it must proceed via amino radical (NH_2), which can further react with atomic hydrogen, leading to the formation of ammonia. These general findings are in agreement with the results of Liu et al.[83] However, some discrepancies were found between the previously reported pathways (path-2 and path-4) and our current study, as summarized in Table 4.

Although path-2 of Liu's DFT study corresponds to NH_2-I of the present work (Figure 7, above), our calculations show one additional step before the formation of amino radical, involving a previously unreported five-membered ring disassembly (TS25) before the formation of the NH_2 group (TS190, matching the previous in-2-2t) in the intermediate MIN12 (2-ethynylaniline).

As for path-4, its second step (TS17 in this work, 4-2t in ref 83) would be a self-loop connecting MIN12 (4-2m) with itself. Therefore, this path will not contribute to the formation of amino radical or ammonia. Instead, we propose a new channel (NH_2-II) comprising two grouped pathways for NH_2 radical formation (Figure 7, below). Despite their larger activation energies, these two paths are one step shorter than NH_2-I and might be kinetically competitive.

3.5. Implications in Astrochemistry

One of the possible applications of the newly developed tools could be the quest for barrierless gas-phase reactions yielding complex organic molecules detected in the ISM, which are

https://doi.org/10.1021/acsphyschemau.1c00051
ACS Phys. Chem Au 2022, 2, 225−236

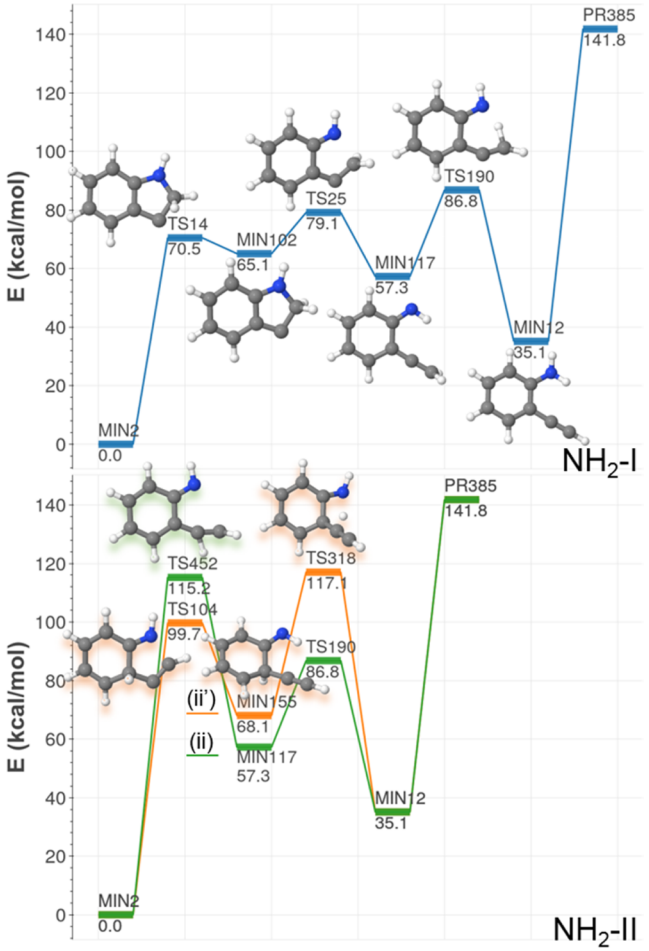

Figure 7. Level3-calculated energy profiles for the NH_2 elimination pathways from indole found in this study. The channels were obtained after filtering those obtained at Level2 using a threshold energy of 150 kcal/mol and a maximum number of elementary steps of 4.

Table 4. NH_3 Formation Pathways (via NH_2 Radical) Predicted by AutoMeKin in Comparison with the Previous DFT Study

Liu et al.[83]	this work[a]
Path-2[b]	NH_2-I
Path-4[b]	
[c]	NH_2-II (*x2*)

[a]Pathways are named FRAG(-*a*-)-X, where FRAG is the chemical formula of the obtained fragment, X is a Roman numeral, and -a- refers to indole-a. Labels of products (PR) and minima (MIN) correspond to the RXNet obtained at Level3 from indole/indole-a. [b]Previous IRC characterizations on the path do not match current calculations (see text for more details). [c]Not found in the previous DFT study.

usually called interstellar complex organic molecules (iCOMs).[109] Several formation mechanisms of iCOMs are possible, but neutral gas-phase reactions probably play an important role.[110] Due to the very low temperatures of the ISM, these mechanisms should occur barrierlessly, i.e., with the energy of reactants being above the highest TS in the energy profile.[64]

The first step of the procedure described in this section consists of identifying the molecules that can initiate the process. An analysis of the list of fragments obtained in the decomposition of indole affords two potential candidates: methylene radical and phenyl isocyanide (C_6H_5NC). The former has been already detected in the ISM.[86] Besides, the recent detection of benzonitrile (C_6H_5CN)[87] in the molecular cloud TMC-1 suggests the consideration of the isomeric phenyl isocyanide.[111] Furthermore, previous work showed that the formation of phenyl isocyanide is possible from benzene and cyano radical, although at low abundances relative to benzonitrile.[112]

After this preliminary analysis, we set out to seek a barrierless mechanism for the formation of indole. Figure 8

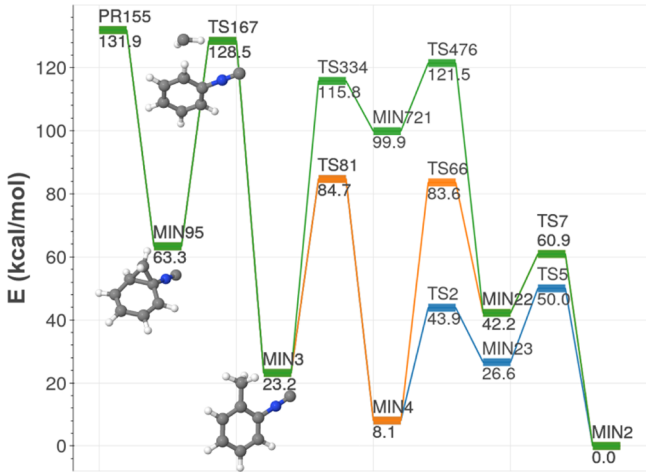

Figure 8. Level3-calculated energy profile for the barrierless indole formation mechanism found in this study from methylene and phenyl isocyanide. The reactants (methylene and phenyl isocyanide) are tagged as PR155 because the fragmentation (rather than the formation) of indole was studied.

shows the only mechanism found in this study connecting methylene and phenyl isocyanide with indole. The mechanism happened to be barrierless with respect to the reactants (CH_2 and C_6H_5NC), which makes it a plausible route for indole formation in cold and low-pressure environments.[113]

A relaxed scan carried out at the M06-2X/MG3S level of theory confirms that the association of methylene and phenyl isocyanide to form the bicyclic product MIN95 proceeds without a barrier (see Figure S6). The highest energy barrier in the energy profile of Figure 8 corresponds to TS167, which connects the intermediate MIN95 with MIN3 (2-methyl-benzonitrile). The latter is one of the hubs of the RXNet appearing in other pathways (e.g., HNC-II, in Figure 5) and participating in 15 elementary steps. The potential energy surface around TS167 is very flat (see Figure S7) in the direction of MIN95 and its energy is only 3.4 kcal/mol below the reactants. This means that, with the right orientation of the reactants, the association of methylene and phenyl isocyanide might lead to the direct formation of MIN3 skipping past the bicyclic structure MIN95. Similar dynamics effects of a single transition state serving two mechanisms have been found in previous work.[114,115] If this sort of nonstatistical behavior was also confirmed for TS167, the formation of indole would be accelerated for the fraction of trajectories that avoid MIN95. This could be ascertained by running quasi-classical trajectory simulations for the methylene capture step.

The remaining steps leading to indole from MIN3 are already shown in Figure 5 and involve relatively lower barriers.

https://doi.org/10.1021/acsphyschemau.1c00051
ACS Phys. Chem Au 2022, 2, 225−236

The analysis of our RXNet provides a feasible mechanism for indole formation at the very low temperatures (and gas densities) of the ISM, provided phenyl isocyanide is also present in the ISM.

Aside from the suggested formation route, photolysis of indole can lead to HCN after internal conversion to the ground electronic state.[88,89] Furthermore, this triatomic molecule has been detected in the ISM[90] with HNC/HCN branching ratios which are many orders of magnitude higher than the expected one at equilibrium ($\sim 10^{-33}$ at 100 K).[91,92] Motivated by this discrepancy, several molecules have been proposed as viable photolytic sources of HCN and HNC in the ISM with measured/calculated HNC/HCN branching ratios in the range 0.1−0.3.[75,77,116,117]

Table 2 shows that indole can also form both isomers with HCN formation being the predominant mechanism. The table collects the product yields at four different excitation energies. The lowest and highest energies correspond to a photon wavelength of 193 nm and to the Lyman-α wavelength. Our computed HNC/HCN branching ratios range from 0 to 0.003, which is many orders of magnitude greater than the equilibrium value and somehow smaller than the deduced ratio of 0.06 after detecting HCN and HNC in comet C/1996 B2 (Hyakutake).[92] Furthermore, it must be noted that these results do not take into account pathways with energy barriers above 150 kcal/mol, which probably contribute to the branching ratios at the highest excitation energies.

At any rate, our goal with this section is to demonstrate the utility of our current pipeline to help with the identification of formation routes of iCOMs, as well as probing specific dissociation channels of these molecules.

4. CONCLUSIONS

The unimolecular decomposition of indole and its radical resulting from N−H dissociation has been explored through the amk-tools library, a novel Python package designed to parse, process, and transform the reaction networks explored by the automated reaction mechanism discovery tool AutoMeKin. The system was chosen on account of the complexity of the reaction network, involving thousands of stationary points, and the wealth of different dissociation channels, posing a real challenge for the newly developed package. The use of this tool greatly facilitated the analysis of results, integrating in a single dashboard the "big-picture" view provided by the overall reaction network with the specific details (energy, geometry, and vibrational modes) of all intermediates and transition states. The network filtering and reaction path generation capabilities of our code, combined with the kinetic analysis algorithms in the main program, provide a robust way to highlight the chemically relevant sections of complex networks, such as our target unimolecular indole decomposition. Moreover, the integration with the ioChem-BD platform and the generation of dashboards as standalone HTML documents allows AutoMeKin results to be easily shared with other scientists, in line with the FAIR principles for digital data management. The main conclusions of our computational study on the unimolecular decomposition of indole are summarized below.

(a) Nine novel pathways for direct HCN/HNC elimination from indole and indole radical have been proposed.

(b) Regarding CN elimination processes, all of the previously reported channels (three) from indole and its radical are reproduced and six new routes are proposed.

(c) The previously reported amino radical formation mechanisms have been corrected, proposing three different pathways for which both path lengths and path energies must be taken into account.

(d) A feasible barrierless mechanism for indole formation in cold environments is also proposed here. The route might be viable under the very low temperatures and gas densities of the ISM so long as phenyl isocyanide is present in those environments.

(e) The finding of dissociation pathways leading to HCN and HNC isomers opens the possibility that photolysis of indole can help explain the unexpected abundance of HNC with respect to HCN present in the ISM.

(f) The mechanisms reported here can help improve the kinetic models employed to study the pyrolysis of the molecule or in astrochemical models. Regarding the former, our RXNets could be further investigated to include pathways other than those discussed here (like those leading to acetylene or choosing less constrained cutoffs) in a simple manner through the presented network processing tools.

■ ASSOCIATED CONTENT

Supporting Information

The Supporting Information is available free of charge at https://pubs.acs.org/doi/10.1021/acsphyschemau.1c00051.

Additional energy profiles for CN, HCN, and NH_2 formation channels; further characterization of the indole formation route from methylene and phenyl isocyanide (relaxed PES scan and IRC for TS167); example screenshots for the interactive dashboards produced by amk-tools; and details on the barrierless TS search workflow implemented in the last release of AutoMeKin (PDF)

■ AUTHOR INFORMATION

Corresponding Authors

Carles Bo − *Institute of Chemical Research of Catalonia (ICIQ), Barcelona Institute of Science & Technology (BIST), 43007 Tarragona, Spain; Departament de Química Física i Inorgànica, Universitat Rovira i Virgili (URV), 43007 Tarragona, Spain;* orcid.org/0000-0001-9581-2922; Email: cbo@iciq.cat

Emilio Martínez-Núñez − *Departmento de Química Física, Facultade de Química, Universidade de Santiago de Compostela, 15782 Santiago de Compostela, Spain;* orcid.org/0000-0001-6221-4977; Email: emilio.nunez@usc.es

Authors

Diego Garay-Ruiz − *Institute of Chemical Research of Catalonia (ICIQ), Barcelona Institute of Science & Technology (BIST), 43007 Tarragona, Spain; Departament de Química Física i Inorgànica, Universitat Rovira i Virgili (URV), 43007 Tarragona, Spain;* orcid.org/0000-0003-0744-0562

Moises Álvarez-Moreno − *Institute of Chemical Research of Catalonia (ICIQ), Barcelona Institute of Science & Technology (BIST), 43007 Tarragona, Spain*

https://doi.org/10.1021/acsphyschemau.1c00051
ACS Phys. Chem Au 2022, 2, 225−236

Complete contact information is available at:
https://pubs.acs.org/10.1021/acsphyschemau.1c00051

Author Contributions

The manuscript was written through contributions of all authors. All authors have given approval to the final version of the manuscript.

Notes

The authors declare no competing financial interest.
All Level3 calculations at the CCSD(T)/aug-cc-pVTZ//M06-2X/MG3S level for indole and indole-a decompositions are available as a dataset collection in the ioChem-BD repository[95] and can be accessed at http://dx.doi.org/10.19061/iochem-bd-1-223.

■ ACKNOWLEDGMENTS

This work was partially supported by: the Spanish Ministerio de Ciencia e Innovación through Projects PID2019-107307RB-I00 and PID2020-112806RB-I00 and through the Severo Ochoa Excellence Accreditation 2020−2023 (CEX2019-000925-S, MCI/AEI), the Consellería de Cultura, Educación e Ordenación Universitaria e da Consellería de Economía, Emprego e Industria (Axuda para Consolidación e Estructuración de Unidades de Investigación Competitivas do Sistema Universitario de Galicia, Xunta de Galicia ED431C 2021/40), the ICIQ Foundation, and the CERCA Program of the Generalitat de Catalunya. D.G.-R. thanks AGAUR, the Secretaria d'Universitats i Recerca of the Generalitat de Catalunya, and the European Social Fund for a FI predoctoral grant. The authors acknowledge CESGA for providing access to their computing facilities.

■ REFERENCES

(1) Davis, H. L.; Wales, D. J.; Berry, R. S. Exploring potential energy surfaces with transition state calculations. *J. Chem. Phys.* **1990**, *92*, 4308−4319.
(2) Sun, J. Q.; Ruedenberg, K. Gradient Extremals and Steepest Descent Lines on Potential Energy Surfaces. *J. Chem. Phys.* **1993**, *98*, 9707−9714.
(3) Tsai, C. J.; Jordan, K. D. Use of an eigenmode method to locate the stationary points on the potential energy surfaces of selected argon and water clusters. *J. Phys. Chem. A* **1993**, *97*, 11227−11237.
(4) Abashkin, Y.; Russo, N. Transition state structures and reaction profiles from constrained optimization procedure. Implementation in the framework of density functional theory. *J. Chem. Phys.* **1994**, *100*, 4477−4483.
(5) Bondensgård, K.; Jensen, F. Gradient Extremal Bifurcation and Turning Points: an Application to the H_2CO Potential Energy Surface. *J. Chem. Phys.* **1996**, *104*, 8025−8031.
(6) Doye, J. P. K.; Wales, D. J. Surveying a potential energy surface by eigenvector-following. *Z. Phys. D* **1997**, *40*, 194−197.
(7) Quapp, W.; Hirsch, M.; Imig, O.; Heidrich, D. Searching for Saddle Points of Potential Energy Surfaces by Following a Reduced Gradient. *J. Comput. Chem.* **1998**, *19*, 1087−1100.
(8) Černohorský, M.; Kettou, S.; Koča, J. VADER: New Software for Exploring Interconversions on Potential Energy Surfaces. *J. Chem. Inf. Comput. Sci.* **1999**, *39*, 705−712.
(9) Westerberg, K. M.; Floudas, C. A. Locating all transition states and studying the reaction pathways of potential energy surfaces. *J. Chem. Phys.* **1999**, *110*, 9259−9295.
(10) Irikura, K. K.; Johnson, R. D. Predicting unexpected chemical reactions by isopotential searching. *J. Phys. Chem. A* **2000**, *104*, 2191−2194.
(11) Wales, D. J.; Doye, J. P.; Miller, M. A.; Mortenson, P. N.; Walsh, T. R. Energy Landscapes: From Clusters to Biomolecules. *Adv. Chem. Phys.* **2000**, *115*, 1−111.
(12) Dallos, M.; Lischka, H.; Ventura Do Monte, E.; Hirsch, M.; Quapp, W. Determination of Energy Minima and Saddle Points Using Multireference Configuration Interaction Methods in Combination with Reduced Gradient Following: The S_0 surface of H_2CO and the T_1 and T_2 surfaces of acetylene. *J. Comput. Chem.* **2002**, *23*, 576−583.
(13) Müller, E. M.; Meijere, A.; Grubmüller, H. Predicting unimolecular chemical reactions: Chemical flooding. *J. Chem. Phys.* **2002**, *116*, 897−905.
(14) Ohno, K.; Maeda, S. A Scaled Hypersphere Search Method for the Topography of Reaction Pathways on the Potential Energy Surface. *Chem. Phys. Lett.* **2004**, *384*, 277−282.
(15) Baker, J.; Wolinski, K. Isomerization of stilbene using enforced geometry optimization. *J. Comput. Chem.* **2011**, *32*, 43−53.
(16) Schlegel, H. B. Geometry optimization. *Wiley Interdiscip. Rev. Comput. Mol. Sci.* **2011**, *1*, 790−809.
(17) Maeda, S.; Ohno, K.; Morokuma, K. Systematic exploration of the mechanism of chemical reactions: the global reaction route mapping (GRRM) strategy using the ADDF and AFIR methods. *Phys. Chem. Chem. Phys.* **2013**, *15*, 3683−3701.
(18) Zimmerman, P. Reliable Transition State Searches Integrated with the Growing String Method. *J. Chem. Theory Comput.* **2013**, *9*, 3043−3050.
(19) Zimmerman, P. M. Growing string method with interpolation and optimization in internal coordinates: Method and examples. *J. Chem. Phys.* **2013**, *138*, No. 184102.
(20) Bhoorasingh, P. L.; West, R. H. Transition state geometry prediction using molecular group contributions. *Phys. Chem. Chem. Phys.* **2015**, *17*, 32173−32182.
(21) Wales, D. J. Perspective: Insight into reaction coordinates and dynamics from the potential energy landscape. *J. Chem. Phys.* **2015**, *142*, No. 130901.
(22) Zimmerman, P. M. Single-ended transition state finding with the growing string method. *J. Comput. Chem.* **2015**, *36*, 601−611.
(23) Jafari, M.; Zimmerman, P. M. Reliable and efficient reaction path and transition state finding for surface reactions with the growing string method. *J. Comput. Chem.* **2017**, *38*, 645−658.
(24) Broadbelt, L. J.; Stark, S. M.; Klein, M. T. Computer Generated Pyrolysis Modeling: On-the-Fly Generation of Species, Reactions, and Rates. *Ind. Eng. Chem. Res.* **1994**, *33*, 790−799.
(25) Matheu, D. M.; Dean, A. M.; Grenda, J. M.; Green, W. H. Mechanism Generation with Integrated Pressure Dependence: A New Model for Methane Pyrolysis. *J. Phys. Chem. A* **2003**, *107*, 8552−8565.
(26) Maeda, S.; Ohno, K. Global Mapping of Equilibrium and Transition Structures on Potential Energy Surfaces by the Scaled Hypersphere Search Method: Applications to ab Initio Surfaces of Formaldehyde and Propyne Molecules. *J. Phys. Chem. A* **2005**, *109*, 5742−5753.
(27) Ohno, K.; Maeda, S. Global Reaction Route Mapping on Potential Energy Surfaces of Formaldehyde, Formic Acid, and Their Metail-Substituted Analogues. *J. Phys. Chem. A* **2006**, *110*, 8933−8941.
(28) Zimmermann, S.; Urbassek, H. M. Hyperthermal cluster-surface scattering: Comparison of fragmentation, energy redistribution, and sticking in atomic and molecular clusters. *Eur. Phys. J. D* **2006**, *39*, 423.
(29) Ohno, K.; Maeda, S. Automated Exploration of Reaction Channels. *Phys. Scr.* **2008**, *78*, No. 058122.
(30) Maeda, S.; Morokuma, K. Communications: A systematic method for locating transition structures of A+B→X type reactions. *J. Chem. Phys.* **2010**, *132*, No. 241102.
(31) Maeda, S.; Morokuma, K. Finding Reaction Pathways of Type A + B → X: Toward Systematic Prediction of Reaction Mechanisms. *J. Chem. Theory Comput.* **2011**, *7*, 2335−2345.

(32) Zimmerman, P. M. Automated discovery of chemically reasonable elementary reaction steps. *J. Comput. Chem.* **2013**, *34*, 1385−1392.
(33) Maeda, S.; Taketsugu, T.; Morokuma, K. Exploring transition state structures for intramolecular pathways by the artificial force induced reaction method. *J. Comput. Chem.* **2014**, *35*, 166−173.
(34) Rappoport, D.; Galvin, C. J.; Zubarev, D. Y.; Aspuru-Guzik, A. Complex Chemical Reaction Networks from Heuristics-Aided Quantum Chemistry. *J. Chem. Theory Comput.* **2014**, *10*, 897−907.
(35) Schaefer, B.; Mohr, S.; Amsler, M.; Goedecker, S. Minima hopping guided path search: An efficient method for finding complex chemical reaction pathways. *J. Chem. Phys.* **2014**, *140*, No. 214102.
(36) Wang, L.-P.; Titov, A.; McGibbon, R.; Liu, F.; Pande, V. S.; Martínez, T. J. Discovering chemistry with an ab initio nanoreactor. *Nat. Chem.* **2014**, *6*, 1044−1048.
(37) Bergeler, M.; Simm, G. N.; Proppe, J.; Reiher, M. Heuristics-Guided Exploration of Reaction Mechanisms. *J. Chem. Theory Comput.* **2015**, *11*, 5712−5722.
(38) Habershon, S. Sampling reactive pathways with random walks in chemical space: Applications to molecular dissociation and catalysis. *J. Chem. Phys.* **2015**, *143*, No. 094106.
(39) Martínez-Núñez, E. An automated transition state search using classical trajectories initialized at multiple minima. *Phys. Chem. Chem. Phys.* **2015**, *17*, 14912−14921.
(40) Martínez-Núñez, E. An automated method to find transition states using chemical dynamics simulations. *J. Comput. Chem.* **2015**, *36*, 222−234.
(41) Suleimanov, Y. V.; Green, W. H. Automated Discovery of Elementary Chemical Reaction Steps Using Freezing String and Berny Optimization Methods. *J. Chem. Theory Comput.* **2015**, *11*, 4248−4259.
(42) Zhang, X.-J.; Liu, Z.-P. Reaction sampling and reactivity prediction using the stochastic surface walking method. *Phys. Chem. Chem. Phys.* **2015**, *17*, 2757−2769.
(43) Zimmerman, P. M. Navigating molecular space for reaction mechanisms: an efficient, automated procedure. *Mol. Simul.* **2015**, *41*, 43−54.
(44) Habershon, S. Automated Prediction of Catalytic Mechanism and Rate Law Using Graph-Based Reaction Path Sampling. *J. Chem. Theory Comput.* **2016**, *12*, 1786−1798.
(45) Maeda, S.; Harabuchi, Y.; Takagi, M.; Taketsugu, T.; Morokuma, K. Artificial Force Induced Reaction (AFIR) Method for Exploring Quantum Chemical Potential Energy Surfaces. *Chem. Rec.* **2016**, *16*, 2232−2248.
(46) Proppe, J.; Husch, T.; Simm, G. N.; Reiher, M. Uncertainty quantification for quantum chemical models of complex reaction networks. *Faraday Discuss.* **2016**, *195*, 497−520.
(47) Wang, L.-P.; McGibbon, R. T.; Pande, V. S.; Martinez, T. J. Automated Discovery and Refinement of Reactive Molecular Dynamics Pathways. *J. Chem. Theory Comput.* **2016**, *12*, 638−649.
(48) Dewyer, A. L.; Zimmerman, P. M. Finding reaction mechanisms, intuitive or otherwise. *Org. Biomol. Chem.* **2017**, *15*, 501−504.
(49) Jacobson, L. D.; Bochevarov, A. D.; Watson, M. A.; Hughes, T. F.; Rinaldo, D.; Ehrlich, S.; Steinbrecher, T. B.; Vaitheeswaran, S.; Philipp, D. M.; Halls, M. D.; Friesner, R. A. Automated Transition State Search and Its Application to Diverse Types of Organic Reactions. *J. Chem. Theory Comput.* **2017**, *13*, 5780−5797.
(50) Maeda, S.; Harabuchi, Y.; Takagi, M.; Saita, K.; Suzuki, K.; Ichino, T.; Sumiya, Y.; Sugiyama, K.; Ono, Y. Implementation and performance of the artificial force induced reaction method in the GRRM17 program. *J. Comput. Chem.* **2018**, *39*, 233−250.
(51) Simm, G. N.; Reiher, M. Context-Driven Exploration of Complex Chemical Reaction Networks. *J. Chem. Theory Comput.* **2017**, *13*, 6108−6119.
(52) Varela, J. A.; Vazquez, S. A.; Martinez-Nunez, E. An automated method to find reaction mechanisms and solve the kinetics in organometallic catalysis. *Chem. Sci.* **2017**, *8*, 3843−3851.
(53) Yang, M.; Zou, J.; Wang, G.; Li, S. Automatic Reaction Pathway Search via Combined Molecular Dynamics and Coordinate Driving Method. *J. Phys. Chem. A* **2017**, *121*, 1351−1361.
(54) Dewyer, A. L.; Argüelles, A. J.; Zimmerman, P. M. Methods for exploring reaction space in molecular systems. *WIREs Comput. Mol. Sci.* **2018**, *8*, No. e1354.
(55) Kim, Y.; Kim, J. W.; Kim, Z.; Kim, W. Y. Efficient prediction of reaction paths through molecular graph and reaction network analysis. *Chem. Sci.* **2018**, *9*, 825−835.
(56) Simm, G. N.; Reiher, M. Error-Controlled Exploration of Chemical Reaction Networks with Gaussian Processes. *J. Chem. Theory Comput.* **2018**, *14*, 5238−5248.
(57) Vázquez, S. A.; Otero, X. L.; Martinez-Nunez, E. A Trajectory-Based Method to Explore Reaction Mechanisms. *Molecules* **2018**, *23*, No. 3156.
(58) Ismail, I.; Stuttaford-Fowler, H. B. V. A.; Ochan Ashok, C.; Robertson, C.; Habershon, S. Automatic Proposal of Multistep Reaction Mechanisms using a Graph-Driven Search. *J. Phys. Chem. A* **2019**, *123*, 3407−3417.
(59) Kawano, M.; Koido, S.; Nakatomi, T.; Watabe, Y.; Takayanagi, T. Automated reaction path search calculations of spin-inversion mechanisms in the 6,4,2Nb + C2H4 reaction. *Comput. Theor. Chem.* **2019**, *1155*, 31−37.
(60) Robertson, C.; Habershon, S. Fast screening of homogeneous catalysis mechanisms using graph-driven searches and approximate quantum chemistry. *Catal. Sci. Technol.* **2019**, *9*, 6357−6369.
(61) Simm, G. N.; Vaucher, A. C.; Reiher, M. Exploration of Reaction Pathways and Chemical Transformation Networks. *J. Phys. Chem. A* **2019**, *123*, 385−399.
(62) Jara-Toro, R. A.; Pino, G. A.; Glowacki, D. R.; Shannon, R. J.; Martínez-Núñez, E. Enhancing Automated Reaction Discovery with Boxed Molecular Dynamics in Energy Space. *ChemSystemsChem* **2020**, *2*, No. e1900024.
(63) Robertson, C.; Ismail, I.; Habershon, S. Traversing Dense Networks of Elementary Chemical Reactions to Predict Minimum-Energy Reaction Mechanisms. *ChemSystemsChem* **2020**, *2*, No. e1900047.
(64) Robertson, C.; Hyland, R.; Lacey, A. J. D.; Havens, S.; Habershon, S. Identifying Barrierless Mechanisms for Benzene Formation in the Interstellar Medium Using Permutationally Invariant Reaction Discovery. *J. Chem. Theory Comput.* **2021**, *17*, 2307−2322.
(65) Young, T. A.; Silcock, J. J.; Sterling, A. J.; Duarte, F. autodE: Automated Calculation of Reaction Energy Profiles— Application to Organic and Organometallic Reactions. *Angew. Chem., Int. Ed.* **2021**, *60*, 4266−4274.
(66) Martínez-Núñez, E.; Barnes, G. L.; Glowacki, D. R.; Kopec, S.; Peláez, D.; Rodríguez, A.; Rodríguez-Fernández, R.; Shannon, R. J.; Stewart, J. J. P.; Tahoces, P. G.; Vazquez, S. A. AutoMeKin2021: An open-source program for automated reaction discovery. *J. Comput. Chem.* **2021**, *42*, 2036−2048.
(67) Shannon, R. J.; Martínez-Núñez, E.; Shalashilin, D. V.; Glowacki, D. R. ChemDyME: Kinetically Steered, Automated Mechanism Generation through Combined Molecular Dynamics and Master Equation Calculations. *J. Chem. Theory Comput.* **2021**, *17*, 4901−4912.
(68) Döntgen, M.; Przybylski-Freund, M.-D.; Kröger, L. C.; Kopp, W. A.; Ismail, A. E.; Leonhard, K. Automated Discovery of Reaction Pathways, Rate Constants, and Transition States Using Reactive Molecular Dynamics Simulations. *J. Chem. Theory Comput.* **2015**, *11*, 2517−2524.
(69) Maeda, S.; Harabuchi, Y.; Takagi, M.; Saita, K.; Suzuki, K.; Ichino, T.; Sumiya, Y.; Sugiyama, K.; Ono, Y. Implementation and performance of the artificial force induced reaction method in the GRRM17 program. *J. Comput. Chem.* **2018**, *39*, 233−251.
(70) Van de Vijver, R.; Zádor, J. KinBot: Automated stationary point search on potential energy surfaces. *Comput. Phys. Commun.* **2020**, *248*, No. 106947.

https://doi.org/10.1021/acsphyschemau.1c00051
ACS Phys. Chem Au 2022, 2, 225−236

(71) Gao, C. W.; Allen, J. W.; Green, W. H.; West, R. H. Reaction Mechanism Generator: Automatic construction of chemical kinetic mechanisms. *Comput. Phys. Commun.* **2016**, *203*, 212−225.
(72) Ferro-Costas, D.; Martínez-Núñez, E.; Rodríguez-Otero, J.; Cabaleiro-Lago, E.; Estévez, C. M.; Fernández, B.; Fernández-Ramos, A.; Vázquez, S. A. Influence of Multiple Conformations and Paths on Rate Constants and Product Branching Ratios. Thermal Decomposition of 1-Propanol Radicals. *J. Phys. Chem. A* **2018**, *122*, 4790−4800.
(73) Fenard, Y.; Gil, A.; Vanhove, G.; Carstensen, H.-H.; Van Geem, K. M.; Westmoreland, P. R.; Herbinet, O.; Battin-Leclerc, F. A model of tetrahydrofuran low-temperature oxidation based on theoretically calculated rate constants. *Combust. Flame* **2018**, *191*, 252−269.
(74) Esteban, A.; Izquierdo, I.; García, N.; Sexmero, M. J.; Garrido, N. M.; Marcos, I. S.; Sanz, F.; Jambrina, P. G.; Ortega, P.; Diez, D. Asymmetric [3+2] cycloaddition reaction of a chiral cyclic nitrone for the synthesis of new tropane alkaloids. *Tetrahedron* **2020**, *76*, No. 130764.
(75) Wilhelm, M. J.; Martínez-Núñez, E.; González-Vázquez, J.; Vázquez, S. A.; Smith, J. M.; Dai, H.-L. Is Photolytic Production a Viable Source of HCN and HNC in Astrophysical Environments? A Laboratory-based Feasibility Study of Methyl Cyanoformate. *Astrophys. J.* **2017**, *849*, No. 15.
(76) Pérez-Soto, R.; Vazquez, S. A.; Martinez-Nunez, E. Photodissociation of acryloyl chloride at 193 nm: interpretation of the product energy distributions, and new elimination pathways. *Phys. Chem. Chem. Phys.* **2016**, *18*, 5019−5026.
(77) Vázquez, S. A.; Martinez-Nunez, E. HCN elimination from vinyl cyanide: product energy partitioning, the role of hydrogen-deuterium exchange reactions and a new pathway. *Phys. Chem. Chem. Phys.* **2015**, *17*, 6948−6955.
(78) da Silva, F. F.; Cunha, T.; Rebelo, A.; Gil, A.; Calhorda, M. J.; García, G.; Ingólfsson, O.; Limão-Vieira, P. Electron-Transfer-Induced Side-Chain Cleavage in Tryptophan Facilitated through Potassium-Induced Transition-State Stabilization in the Gas Phase. *J. Phys. Chem. A* **2021**, *125*, 2324−2333.
(79) Rossich Molina, E.; Salpin, J.-Y.; Spezia, R.; Martinez-Nunez, E. On the gas phase fragmentation of protonated uracil: a statistical perspective. *Phys. Chem. Chem. Phys.* **2016**, *18*, 14980−14990.
(80) Macaluso, V.; Scuderi, D.; Crestoni, M. E.; Fornarini, S.; Corinti, D.; Dalloz, E.; Martinez-Nunez, E.; Hase, W. L.; Spezia, R. l-Cysteine Modified by S-Sulfation: Consequence on Fragmentation Processes Elucidated by Tandem Mass Spectrometry and Chemical Dynamics Simulations. *J. Phys. Chem. A* **2019**, *123*, 3685−3696.
(81) Song, L.; Zhang, C.; Sun, C.-G.; Hu, B.-C.; Ju, X.-H. Stabilization mechanisms of three novel full-nitrogen molecules. *Monatsh. Chem.* **2021**, *152*, 421−430.
(82) Shui, H.; Zhou, Y.; Li, H.; Wang, Z.; Lei, Z.; Ren, S.; Pan, C.; Wang, W. Thermal dissolution of Shenfu coal in different solvents. *Fuel* **2013**, *108*, 385−390.
(83) Liu, J.; Zhang, X.; Hu, B.; Lu, Q.; Liu, D.-j.; Dong, C.-q.; Yang, Y.-p. Formation mechanism of HCN and NH3 during indole pyrolysis: A theoretical DFT study. *J. Energy Inst.* **2020**, *93*, 649−657.
(84) Becidan, M.; Skreiberg, Ø.; Hustad, J. E. NOx and N2O Precursors (NH3 and HCN) in Pyrolysis of Biomass Residues. *Energy Fuels* **2007**, *21*, 1173−1180.
(85) Vávra, K.; Luková, K.; Kania, P.; Koucký, J.; Urban, Š. Rotational spectra of indole in the lowest vibrational states. *J. Mol. Spectrosc.* **2019**, *363*, No. 111175.
(86) Polehampton, E. T.; Menten, K. M.; Brünken, S.; Winnewisser, G.; Baluteau, J.-P. Far-infrared detection of methylene. *Astron. Astrophys.* **2005**, *431*, 203−213.
(87) McGuire, B. A.; Burkhardt, A. M.; Kalenskii, S.; Shingledecker, C. N.; Remijan, A. J.; Herbst, E.; McCarthy, M. C. Detection of the aromatic molecule benzonitrile (c-C6H5CN) in the interstellar medium. *Science* **2018**, *359*, 202−205.
(88) Nix, M. G. D.; Devine, A. L.; Cronin, B.; Ashfold, M. N. R. High resolution photofragment translational spectroscopy of the near UV photolysis of indole: Dissociation via the 1πσ* state. *Phys. Chem. Chem. Phys.* **2006**, *8*, 2610−2618.
(89) Sobolewski, A. L.; Domcke, W.; Dedonder-Lardeux, C.; Jouvet, C. Excited-state hydrogen detachment and hydrogen transfer driven by repulsive 1πσ* states: A new paradigm for nonradiative decay in aromatic biomolecules. *Phys. Chem. Chem. Phys.* **2002**, *4*, 1093−1100.
(90) Blackman, G. L.; Brown, R. D.; Godfrey, P. D.; Gunn, H. I. The microwave spectrum of HNC: identification of U90.7. *Nature* **1976**, *261*, 395−396.
(91) Brown, R. D. Deuterium enrichment in interstellar HCN and HNC. *Nature* **1977**, *270*, 39−41.
(92) Irvine, W. M.; Bockelee-Morvan, D.; Lis, D. C.; Matthews, H. E.; Biver, N.; Crovisier, J.; Davies, J. K.; Dent, W. R. F.; Gautier, D.; Godfrey, P. D.; Keene, J.; Lovell, A. J.; Owen, T. C.; Phillips, T. G.; Rauer, H.; Schloerb, F. P.; Senay, M.; Young, K. Spectroscopic evidence for interstellar ices in comet Hyakutake. *Nature* **1996**, *383*, 418−420.
(93) Pieri, E.; Lahana, D.; Chang, A. M.; Aldaz, C. R.; Thompson, K. C.; Martínez, T. J. The non-adiabatic nanoreactor: towards the automated discovery of photochemistry. *Chem. Sci.* **2021**, *12*, 7294−7307.
(94) Rodríguez, A.; Rodríguez-Fernández, R.; Vázquez, S. A.; Barnes, G. L.; Stewart, J. P.; Martínez-Núñez, E. tsscds2018: A code for automated discovery of chemical reaction mechanisms and solving the kinetics. *J. Comput. Chem.* **2018**, *39*, 1922−1930.
(95) Hagberg, A. A.; Shult, D. A.; Swart, P. J. In *Exploring Network Structure, Dynamics, and Function Using NetworkX*, Varoquaux, G.; Vaught, T.; Millman, J., Eds.; 7th Python in Science Conference (SciPy2008), Pasadena, CA, 2008; pp 11−15.
(96) Álvarez-Moreno, M.; De Graaf, C.; López, N.; Maseras, F.; Poblet, J. M.; Bo, C. Managing the computational chemistry big data problem: The ioChem-BD platform. *J. Chem. Inf. Model.* **2015**, *55*, 95−103.
(97) Bo, C.; Maseras, F.; López, N. The role of computational results databases in accelerating the discovery of catalysts. *Nat. Catal.* **2018**, *1*, 809−810.
(98) Garay-Ruiz, D. amk-tools. GitHub Repository, 2021. https://github.com/dgarayr/amk_tools (accessed January 25, 2022).
(99) Bokeh Development Team. Bokeh: Python Library for Interactive Visualization, 2018. http://www.bokeh.org (accessed January 25, 2022).
(100) Stewart, J. J. P. Optimization of parameters for semiempirical methods VI: more modifications to the NDDO approximations and re-optimization of parameters. *J. Mol. Model.* **2013**, *19*, 1−32.
(101) Stewart, J. J. P. *MOPAC2016, Stewart Computational Chemistry*; Colorado Springs: CO, USA, 2022.
(102) Frisch, M. J.; Trucks, G. W.; Schlegel, H. B.; Scuseria, G. E.; Robb, M. A.; Cheeseman, J. R.; Scalmani, G.; Barone, V.; Mennucci, B.; Petersson, G. A.; H, N.; Caricato, M.; Li, X.; Hratchian, H. P.; Izmaylov, A. F.; Bloino, J.; Zheng, G.; Sonnenberg, J. L.; Hada, M.; Ehara, M.; Toyota, K.; Fukuda, R.; Hasegawa, J.; Ishida, M.; Nakajima, T.; Honda, Y.; Kitao, O.; Nakai, H.; Vreven, T.; Montgomery J A, J.; Peralta, J. E.; Ogliaro, F.; Bearpark, M.; Heyd, J. J.; Brothers, E.; Kudin, K. N.; Staroverov, V. N.; Kobayashi, R.; Normand, J.; Raghavachari, K.; Rendell, A.; Burant, J. C.; Iyengar, S. S.; Tomasi, J.; Cossi, M.; Rega, N.; Millam, J. M.; Klene, M.; Knox, J. E.; Cross, J. B.; Bakken, V.; Adamo, C.; Jaramillo, J.; Gomperts, R.; Stratmann, R. E.; Yazyev, O.; Austin, A. J.; Cammi, R.; Pomelli, C.; Ochterski, J. W.; Martin, R. L.; Morokuma, K.; Zakrzewski, V. G.; Voth, G. A.; Salvador, P.; Dannenberg, J. J.; Dapprich, S.; Daniels, A. D.; Farkas, Ö.; Foresman, J. B.; Ortiz, J. V.; Cioslowski, J.; Fox, D. J. *Gaussian 09*, revision A.02; Gaussian Inc.: Wallingford, CT, 2009.
(103) Frisch, M. J.; Trucks, G. W.; Schlegel, H. B.; Scuseria, G. E.; Robb, M. A.; Cheeseman, J. R.; Scalmani, G.; Barone, V.; Petersson, G. A.; Nakatsuji, H.; Li, X.; Caricato, M.; Marenich, A. V.; Bloino, J.; Janesko, B. G.; Gomperts, R.; Mennucci, B.; Hratchian, H. P.; Ortiz, J. V.; Izmaylov, A. F.; Sonnenberg, J. L.; Williams; Ding, F.; Lipparini, F.; Egidi, F.; Goings, J.; Peng, B.; Petrone, A.; Henderson, T.; Ranasinghe, D.; Zakrzewski, V. G.; Gao, J.; Rega, N.; Zheng, G.;

https://doi.org/10.1021/acsphyschemau.1c00051
ACS Phys. Chem Au 2022, 2, 225−236

Liang, W.; Hada, M.; Ehara, M.; Toyota, K.; Fukuda, R.; Hasegawa, J.; Ishida, M.; Nakajima, T.; Honda, Y.; Kitao, O.; Nakai, H.; Vreven, T.; Throssell, K.; Montgomery, J. A., Jr.; Peralta, J. E.; Ogliaro, F.; Bearpark, M. J.; Heyd, J. J.; Brothers, E. N.; Kudin, K. N.; Staroverov, V. N.; Keith, T. A.; Kobayashi, R.; Normand, J.; Raghavachari, K.; Rendell, A. P.; Burant, J. C.; Iyengar, S. S.; Tomasi, J.; Cossi, M.; Millam, J. M.; Klene, M.; Adamo, C.; Cammi, R.; Ochterski, J. W.; Martin, R. L.; Morokuma, K.; Farkas, O.; Foresman, J. B.; Fox, D. J. *Gaussian 16*, rev. C.01; Gaussian Inc.: Wallingford, CT, 2016.

(104) Baer, T.; Hase, W. L. *Unimolecular Reaction Dynamics*; Oxford University Press: Oxford, 1996.

(105) Gillespie, D. T. A general method for numerically simulating the stochastic time evolution of coupled chemical reactions. *J. Comput. Phys.* **1976**, *22*, 403−434.

(106) Laskin, A.; Lifshitz, A. Isomerization and Decomposition of Indole. Experimental Results and Kinetic Modeling. *J. Phys. Chem. A* **1997**, *101*, 7787−7801.

(107) Jacob, P.-M.; Lapkin, A. Statistics of the network of organic chemistry. *React. Chem. Eng.* **2018**, *3*, 102−118.

(108) Morgan, J. W. R.; Mehta, D.; Wales, D. J. Properties of kinetic transition networks for atomic clusters and glassy solids. *Phys. Chem. Chem. Phys.* **2017**, *19*, 25498−25508.

(109) Albert, S.; Albert, K. K.; Lerch, P.; Quack, M. Synchrotron-based highest resolution Fourier transform infrared spectroscopy of naphthalene (C10H8) and indole (C8H7N) and its application to astrophysical problems. *Faraday Discuss.* **2011**, *150*, 71−99.

(110) Skouteris, D.; Balucani, N.; Ceccarelli, C.; Vazart, F.; Puzzarini, C.; Barone, V.; Codella, C.; Lefloch, B. The Genealogical Tree of Ethanol: Gas-phase Formation of Glycolaldehyde, Acetic Acid, and Formic Acid. *Astrophys. J.* **2018**, *854*, No. 135.

(111) Zdanovskaia, M. A.; Esselman, B. J.; Woods, R. C.; McMahon, R. J. The 130−370 GHz rotational spectrum of phenyl isocyanide (C6H5NC). *J. Chem. Phys.* **2019**, *151*, No. 024301.

(112) Lee, K. L. K.; McGuire, B. A.; McCarthy, M. C. Gas-phase synthetic pathways to benzene and benzonitrile: a combined microwave and thermochemical investigation. *Phys. Chem. Chem. Phys.* **2019**, *21*, 2946−2956.

(113) Siebrand, W.; Smedarchina, Z.; Martínez-Núñez, E.; Fernández-Ramos, A. Methanol dimer formation drastically enhances hydrogen abstraction from methanol by OH at low temperature. *Phys. Chem. Chem. Phys.* **2016**, *18*, 22712−22718.

(114) Rodríguez-Fernández, R.; Vázquez, S. A.; Martínez-Núñez, E. Collision-induced dissociation mechanisms of [Li(uracil)]+. *Phys. Chem. Chem. Phys.* **2013**, *15*, 7628−7637.

(115) Bakken, V.; Danovich, D.; Shaik, S.; Schlegel, H. B. A Single Transition State Serves Two Mechanisms: An ab Initio Classical Trajectory Study of the Electron Transfer and Substitution Mechanisms in Reactions of Ketyl Radical Anions with Alkyl Halides. *J. Am. Chem. Soc.* **2001**, *123*, 130−134.

(116) Wilhelm, M. J.; Nikow, M.; Letendre, L.; Dai, H.-L. Photodissociation of vinyl cyanide at 193 nm: Nascent product distributions of the molecular elimination channels. *J. Chem. Phys.* **2009**, *130*, No. 044307.

(117) Homayoon, Z.; Vázquez, S. A.; Rodríguez-Fernández, R.; Martínez-Núñez, E. Ab Initio and RRKM Study of the HCN/HNC Elimination Channels from Vinyl Cyanide. *J. Phys. Chem. A* **2011**, *115*, 979−985.

https://doi.org/10.1021/acsphyschemau.1c00051
ACS Phys. Chem Au 2022, 2, 225−236